



Nonlinear Elastic Waves for Evaluation of Composite Material Deterioration

Rolf LAMMERING, Natalie RAUTER

Institute of Mechanics
Helmut-Schmidt-University/University of the Federal Armed Forces Hamburg
Holstenhofweg 85, 22043 Hamburg, Germany
e-mail: rolf.lammering@hsu-hh.de

This work deals with numerical investigations on nonlinear wave propagation in order to detect micro-damage in composite material. For this purpose two models are under consideration. First, a wave guide with linear-elastic material behavior with and without a crack is analyzed. The nonlinearity of this model is due to the strain tensor as well as the contact of the crack surfaces. Secondly, a hyper-elastic waveguide with a nonlinear constitutive description is considered. It is shown, that the nonlinearity gives rise to second harmonic wave modes which may be considered as an indicator of micro-damage and material deterioration.

Key words: nonlinear elastic waves, composite material, material deterioration, damage.

1. INTRODUCTION

In composite structures cyclic loading leads to micro-structural damage even at an early lifetime stage and thus gives rise to the development of microscopic cracks in the matrix material and fiber/matrix interface debonding. In order to detect this micro-structural damage accurately new methods are currently under investigation. Guided waves, e.g. generated by piezoelectric devices, allow the reliable detection of damage like delaminations [7]. However, the size of micro-structural damage is too small to cause noticeable effects in the wave propagation pattern like mode conversion.

However, methods based on nonlinear elastic waves are promising for the development of appropriate tools which enable the detection of micro-structural damage. These methods make use of the fact that a damaged structure behaves in a nonlinear way. So, a mono-frequent structural excitation causes not only a wave at the respective frequency but also higher harmonic wave modes, [1, 4]. However, their amplitudes are very small so that a cumulative effect has to be

used which ensures growing amplitudes with increasing propagating distance and thus an accurate amplitude determination. To get a better insight into the physics behind this inspection method numerical simulations are essential beside experimental investigations.

This study deals with numerical investigations of a two-dimensional model of a plate in a plane strain state. The nonlinear structural behavior is included in two different ways. First, the micro-structural damage is modeled geometrically by breathing cracks of which the surfaces get into contact when a wave is running through. Subsequently, a novel nonlinear hyper-elastic material model is applied which substitutes Murnaghan's five constant nonlinear elastic theory [3] and which accounts for transverse isotropy. The computations show that both models lead to comparable results.

2. NONLINEAR MODELS

As a first model a structure with and without a crack (length 1 mm, width $70\ \mu\text{m}$) in its midplane is investigated. In any case, aluminum with linear isotropic material behavior is assumed. The numerical set-up is shown in Fig. 1. In the numerical analysis, the non-linearity of the model results from the use of the non-linear Green-Lagrangean strain tensor on the one hand and, additionally, from the contact boundary conditions at the crack surfaces on the other hand.

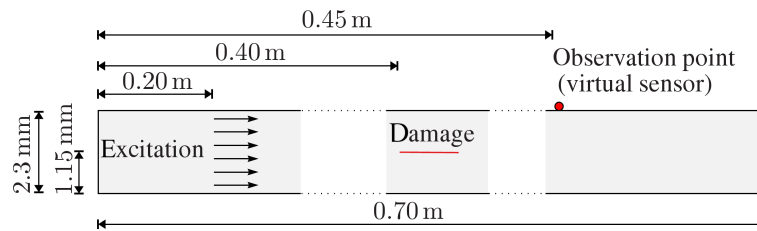


FIG. 1. Numerical model for wave propagation simulation.

The second model is built from a non-damaged plate structure with a nonlinear hyper-elastic material model. The geometry is the similar to the first model, see Fig. 1, however, the length is 0.5 m and the thickness 1 mm. The material is described by a strain energy function Ψ_{tr} which takes into account the transverse isotropic material behavior of a lamina with unidirectional fiber orientation as well as its compressibility, see [5]. The strain energy function Ψ_{tr} is composed of two parts

$$(2.1) \quad \Psi_{\text{tr}} = \Psi_{\text{inc}} + \Psi_{\text{com}}.$$

Here, Ψ_{inc} represents a strain energy function for an incompressible, transverse isotropic material, see [6], which is given by

$$(2.2) \quad \Psi_{\text{inc}} = c_1(I_1 - 3)^2 + c_2(I_2 - 3) - 2c_2(I_1 - 3) + c_3(I_4 - 1)^2 \\ + c_4(I_5 - 1) - 2c_4(I_4 - 1) + c_5(I_4 - 1)(I_1 - 3),$$

and Ψ_{com} accounts for the compressibility, see [2], which is due to the matrix material

$$(2.3) \quad \Psi_{\text{com}} = \frac{K}{4} (J^2 - 1 - 2 \ln J).$$

It should be noted that Ψ_{inc} describes a linear hyper-elastic material model since the resulting elasticity tensor \mathbb{C} is independent of the strain state. However, due to Ψ_{com} , the tensor \mathbb{C} becomes dependent of the strain state \mathbf{C} so that the constitutive Eq. (2.1) is nonlinear. Furthermore, it is pointed out that in total six material constants have to be determined for material description.

3. CUMULATIVE HIGHER HARMONIC WAVE MODES

In a nonlinear medium a mono-frequent excitation causes a structural response not only at the excitation frequency but also at higher harmonic frequencies. The resulting higher harmonic wave modes usually have very small amplitudes. Therefore, they subside very quickly and are difficult to capture in experiments. To overcome this problem and to allow for the accurate detection of higher harmonic wave modes, a cumulative effect is used for which the following conditions have to be satisfied. First, a non-zero power flux from the primary to the second harmonic wave mode has to exist and, secondly, the phase velocity of the primary and second harmonic wave modes have to be equal. In this case, the modes are called internally resonant and the amplitude of the higher harmonic wave grows linearly with the propagation distance. If the phase velocities are different it shows an oscillating behavior with a wavelength depending on the difference of phase velocities.

A third condition, the matching of the group velocities, was controversially discussed in the past. This condition is not necessary for the cumulative effect. However, if the group velocities match both wave modes do not separate and thus the higher harmonic wave does not extend over the covered propagation distance. So, in order to detect the amplitudes of the fundamentally excited and the higher harmonic Lamb wave mode simultaneously this condition is taken into account as a third one for the selection of suitable mode pairs and the determination of the excitation frequency in this study.

For the first model, this procedure is shown exemplarily with the help of Fig. 2. The dispersion diagrams for the phase velocity as well as the group velocity are shown in Figs. 2a and 2b. It becomes visible that the S_1 -mode and

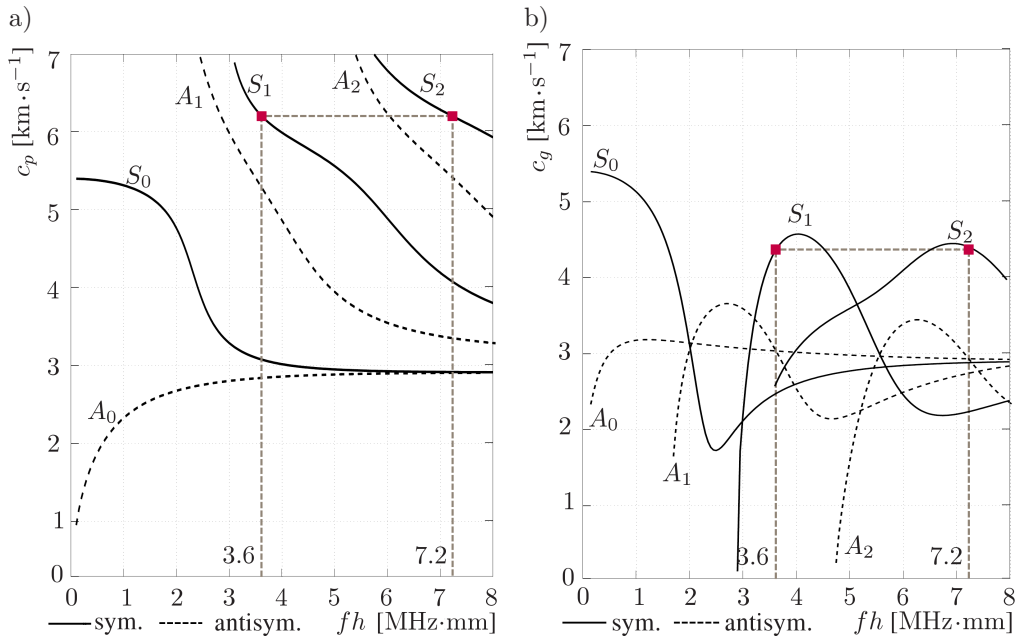


FIG. 2. Excitation frequency for the aluminum specimen at equal phase and group velocities: a) dispersion curves of the phase velocity, b) dispersion curves of the group velocity.

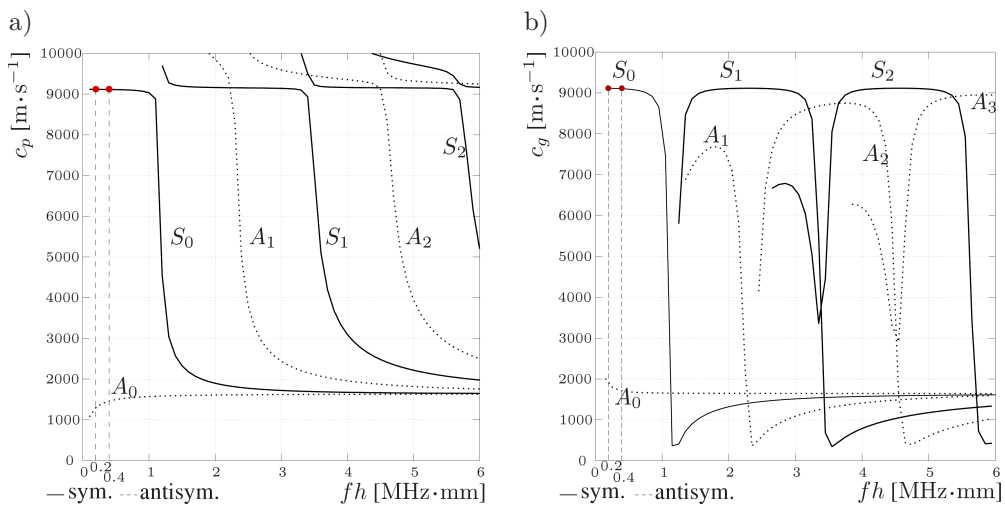


FIG. 3. Dispersion curves for a unidirectional lamina in fiber direction and excitation of S_0 - S_0 -mode pair: a) dispersion curves of the phase velocity, b) dispersion curves of the group velocity.

the S_2 -mode have the same phase and group velocities if the primary S_1 -mode is excited at $fh = 3.6 \text{ MHz} \cdot \text{mm}$ so that second harmonic S_2 -mode is generated at $2fh = 7.2 \text{ MHz} \cdot \text{mm}$, see related marks.

For the transverse isotropic material, dispersion diagrams for the phase velocity as well as the group velocity of the unidirectional lamina are presented in Figs. 3a and 3b. The material parameters necessary for their computations are given in Table 1. This specimen is excited at a frequency of 200 kHz so that the secondary wave is excited at 400 kHz. Since the phase velocities of the primary and secondary waves show a small difference, the amplitude of the secondary wave is oscillating. However, the wavelength of this oscillation is more than 50 m and thus extremely long, see [4].

Table 1. Material parameters of the unidirectional composite.

C_{11}	C_{12}	C_{22}	C_{23}	C_{44}	C_{66}	ρ
122.3 GPa	8.08 GPa	2.38 GPa	5.82 GPa	3.75 GPa	4 GPa	$1.47 \text{ kg} \cdot \text{m}^{-3}$

4. ANALYSIS AND RESULTS

In Fig. 4 some results are shown which are obtained from the first model. The excitation is generated at 1.571 MHz by a windowed sine burst signal of 20 cycles with a maximum amplitude of $0.5 \mu\text{m}$. The in-plane displacements with respect to time at the observation point, see Fig. 1, are presented in Fig. 4a. Three wave packets are visible which are directly generated by the excitation forces. Since the plate is loaded symmetrically the wave packets result from symmetric modes. They are assigned in order of their group velocities as S_1 -, S_2 - and S_0 -modes. Due to their different group velocities the wave packets separate from each other.

In the following, the S_1 -wave mode is under attention. At the selected excitation frequency, the conditions for cumulative higher harmonic wave modes are met and, therefore, a secondary wave field is generated, namely as S_2 -wave mode at twice the excitation frequency. This is confirmed by a FFT analysis of the respective time signal. The result is shown in Fig. 4b from which it becomes obvious that the excitation frequency as well as twice the frequency are included.

Finally, Fig. 4c shows the cumulative effect. Here, the ratio $\tilde{\beta}$ of the amplitudes of both wave modes, which were computed by a wavelet analysis before, is plotted with respect to the propagation distance. It becomes visible that this ratio is rising due to the increasing amplitude of the secondary wave. Further investigations on a waveguide with a single crack show that the generation of the secondary wave mode is increased. This is indicated by the upper curve in

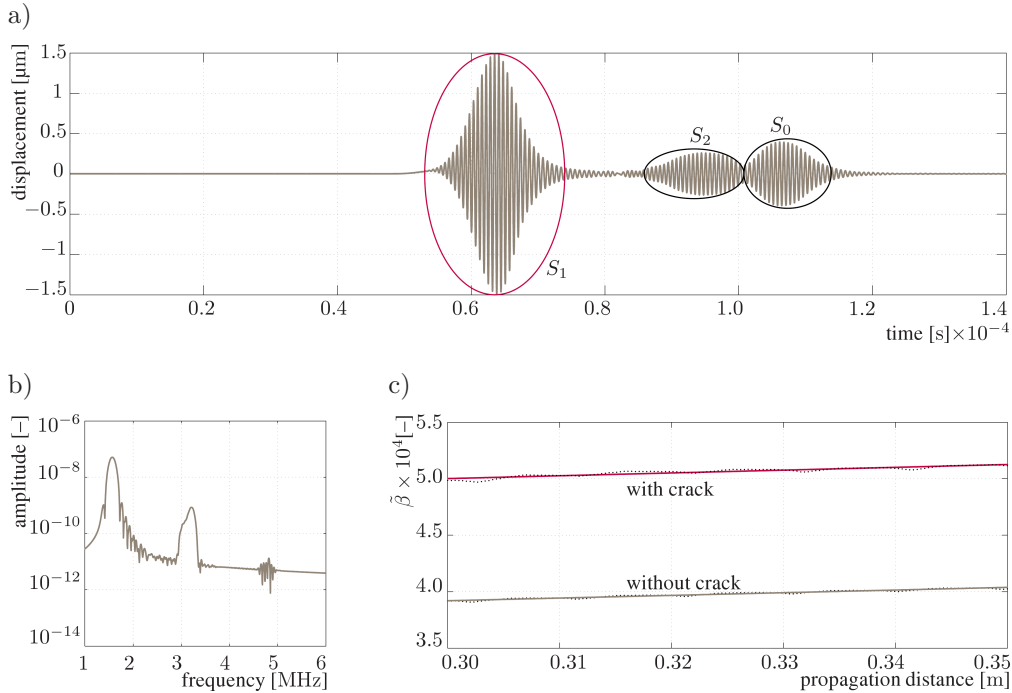


FIG. 4. Wave propagation in a linear-elastic waveguide with primary S_1 -mode and second harmonic S_2 -wave mode at 1.571 MHz and 3.142 MHz, respectively: a) time vs. in-plane displacement at observation point, b) FFT analysis of wave packet 1, c) amplitudes ratio $\tilde{\beta}$ vs. propagation distance with and without crack.

Fig. 4c. Additional computations gave the result that the amplitude ratio $\tilde{\beta}$ is sensitive to the crack length but not to the crack width. In the case of multiple cracks, the longest crack has the main impact on $\tilde{\beta}$ and this parameter becomes not significantly larger in case of further cracks, see [4].

Next, the second model with the hyper-elastic material behavior given by the strain energy function in (2.1) is under investigation. Instead of a cumulative mode pair with phase velocity matching a mode pair without this condition is used, see Fig. 3. In this case the oscillating behavior is analyzed by determining the spatial periodicity of the second harmonic amplitude numerically, see [4]. This analysis is possible for the S_0 - S_0 -mode pair at lower frequencies when the phase velocities do not differ very much. For an excitation frequency of 200 kHz the required element size and time step are much smaller than in the case of high frequency excitation so that the size of the numerical model can be reduced significantly.

Figure 5a shows the displacement with respect to time at the observation point. Since the excitation is at 200 kHz and thus in the low frequency range, only one wave packet is visible. The FFT analysis of this signal is shown

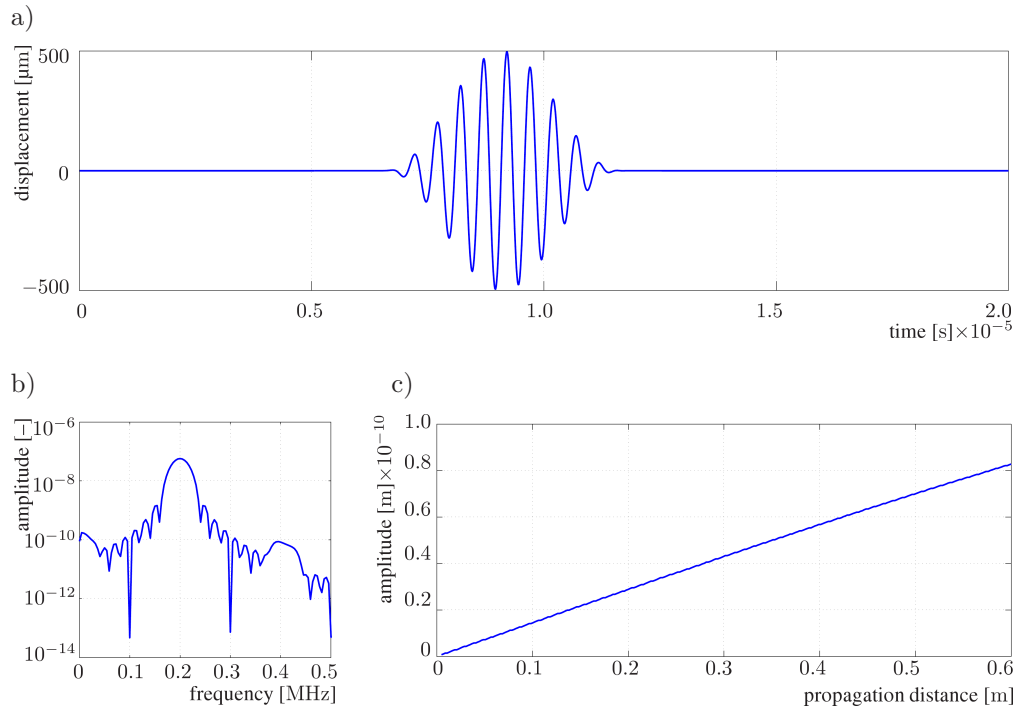


FIG. 5. Wave propagation in a hyper-elastic waveguide with primary S_0 -mode and second harmonic S_0 -wave mode at 200 kHz and 400 kHz, respectively: a) time vs. in-plane displacement at observation point, b) FFT analysis of the wave packet, c) second harmonic amplitude vs. propagation distance.

in Fig. 5b. It is evident that the second harmonic at 400 kHz is included. Finally, Fig. 5c shows that the amplitude of the second harmonic S_0 -mode grows with increasing propagation distance. However, it should be kept in mind that this is the first part of an oscillating curve with a long wavelength.

The bulk modulus K in the nonlinear term (2.3) of the material model in (2.1) influences the amplitude of the second harmonic wave. However, it does not affect its overall behavior along the propagation distance and, therefore, it could be an appropriate measure for the extent of micro-mechanical damage and thus for the material deterioration.

5. CONCLUSIONS

This study shows that a nonlinear hyper-elastic material model allows to simulate the cumulative effect of higher harmonic guided waves. Regarding the wave propagation, the nonlinear material model leads to comparable effects than micro-structural cracks. It may be concluded, that micro-mechanically

damaged material can be modelled by a nonlinear material model with appropriately adapted material parameters in case of wave propagation analysis. Furthermore, these material parameters may give information about the degree of material deterioration. Furthermore, the relative acoustical nonlinearity parameter β' is appropriate for the evaluation of material degradation in composite structures.

REFERENCES

1. CHILLARA V.K., LISSENDEN C.J., *Nonlinear guided waves in plates: a numerical perspective*, Ultrasonics, **54**(6): 1553–1558, 2014.
2. HOLZAPFEL G., *Nonlinear Solid Mechanics – A Continuum Approach for Engineering*, John Wiley & Sons, Inc., 2000.
3. MURNAGHAN F.D., *Finite Deformation of an Elastic Solid*, Dover Publications, New York, 1951.
4. RAUTER N., *Analyse des Einflusses der Werkstoffdegradation auf die nichtlineare Wellenausbreitung in unidirektionalen Compositen – Experimentelle Untersuchung mit numerischer Analyse und Modellbildung*, PhD-Thesis, Institute of Mechanics, Helmut-Schmidt-University/University of the Federal Armed Forces Hamburg, to appear 2017.
5. RAUTER N., LAMMERING R., *Development of a hyper-elastic transversely isotropic material law for the simulation of the higher harmonic Lamb wave generation in composite structures*, Proc. Int. Workshop Struct. Health Monit., Stanford, CA, USA, Sept. 1–3, 2015, 8 pages, 2015.
6. REESE S., RAIBLE T., WRIGGERS P., *Finite element modelling of orthotropic material behaviour in pneumatic membranes*, International Journal of Solids and Structures, **38**(52): 9525–9544, 2001.
7. UNGETHÜM A., LAMMERING R., *Damage localization of carbon fibre reinforced plastic plates*, Proc. Appl. Math. Mech., **10**(1): 19–22, 2010.

Received October 15, 2016; accepted version October 18, 2016.
